Materials and Design 87 (2015) 905–913

Contents lists available at ScienceDirect

Materials and Design

journal homepage: www.elsevier.com/locate/jmad

# Microstructure and mechanical properties of resistance spot welded AZ31/AA5754 using a nickel interlayer

M. Sun [a,b,*], S.T. Niknejad [b], G. Zhang [a,b], M.K. Lee [c], L. Wu [a], Y. Zhou [b]

[a] State Key Laboratory of Advanced Welding and Joining, Harbin Institute of Technology, Harbin 150001, China
[b] Centre for Advanced Materials Joining, University of Waterloo, 200 University Ave., Waterloo, ON N2l 3G1, Canada
[c] Research Institute of Industrial Science & Technology, Pohang 790-600, South Korea

ARTICLE INFO

*Article history:*
Received 6 May 2015
Received in revised form 25 July 2015
Accepted 19 August 2015
Available online 21 August 2015

*Keywords:*
Resistance spot welding
Al AA5754/Mg AZ31B dissimilar welding
Interfacial reaction
Intermetallic compounds
Ni interlayer

ABSTRACT

Dissimilar joining of aluminum (AA5754) and magnesium (AZ31) alloys was investigated in the current study via resistance spot welding. A commercial pure nickel interlayer was inserted between the two base metals to prevent the formation of Al–Mg intermetallic compounds. Microstructural investigations, via SEM/EDS and XRD methods, were carried out to characterize the Mg/Ni and Al/Ni interfaces. It was found that the Al–Mg reaction was successfully prevented and continuous submicron intermetallic layers (through Al–Ni and Mg–Ni reactions) were formed at the separate interfaces. The mechanical test results indicated substantial improvement in the joint strength compared to a direct joint without using an interlayer. The application of excessively high welding current (42 kA) caused microstructure deterioration at the Mg/Ni interfacial region. Investigation of the fracture surface revealed that microstructure defects in the latter region should take responsibility for the reduction in the joint strength at high welding current (42 kA).



## 1. Introduction

There has been a growing interest in using lightweight materials for fabrication of auto-body structures which will contribute to improved fuel efficiency and reduced environmental impacts [1]. In this regard, magnesium and aluminum alloys appear to be good candidates. Therefore, fabrication of hybrid structures of magnesium and aluminum alloys is desirable in many auto-related applications; however direct joints between aluminum and magnesium, produced via thermal processes such as welding, suffer from poor strength and ductility. Such poor mechanical properties are a result of development of brittle intermetallic phase(s), i.e., $Mg_{17}Al_{12}$ and $Al_3Mg_2$ during welding, as already investigated in literatures [2–8]. Thus, in order to achieve a strong joint during fusion welding, direct contact between aluminum and magnesium should be avoided. This can be achieved by inserting an interlayer element at the contact area of the two base materials.

The feasibility of using interlayers such as Cu, Fe, Ce, Ti, Ni and Zn-based alloys in aluminum/magnesium joining has been studied previously and the results have shown that joint strength was improved by using such interlayers [9–18]. For example, successful joining of magnesium to aluminum by resistance spot welding was reported using a gold-coated nickel interlayer [15]; however, the cost of gold coating will restrict the practical applications of this approach.

In the current work, joining of aluminum to magnesium was carried out via resistance spot welding with a commercial pure nickel intermediate layer. Attempts have been made to correlate the bonding strength to microstructural features observed within the reaction zones at magnesium/nickel and aluminum/nickel interfaces.

## 2. Experimental procedures

The materials used in the current work were commercial-grade hot rolled sheets of AZ31B-H24 and AA5754-O with thickness of 2 mm. The chemical compositions, tensile and thermal properties of the as received alloys are shown in Table 1 [19]. Rectangular specimens of 100 mm × 25 mm were prepared for resistance spot welding (RSW) according to AWS-D17.2 standard. A commercial pure nickel foil with a thickness of 0.2 mm was used as an interlayer. The surfaces of all the materials were ultrasonically cleaned in ethanol for 10 min. The surfaces of the aluminum coupons were further cleaned with a solution of 1.2 ml HF, 67.5 ml $HNO_3$ and 100 ml water. And the surfaces of magnesium coupons were further cleaned with a solution of 2.5 g chromic oxide and 100 ml water.

RSW was performed using a medium frequency DC spot welding machine (Centerline Ltd., Windsor, ON, Canada). Initial welding were carried out with the type FF-25 electrodes on both sides (i.e. Mg and Al); however, it was found that insignificant melting took place on the Al side. It is believed that was due to insufficient heat generation. Therefore, the FF-25 electrode tip faces were flattened to have a diameter of 12 mm on the Al side and 16 mm on the Mg side, in order to have better

* Corresponding author at: State Key Laboratory of Advanced Welding and Joining, Harbin Institute of Technology, Harbin 150001, China.
*E-mail address:* sunmeng1239@163.com (M. Sun).

http://dx.doi.org/10.1016/j.matdes.2015.08.097
0264-1275/

**Table 1**
Chemical composition (wt.%), tensile and thermal properties of the as-received alloys.

| | Al | Mg | Mn | Zn | Fe | Si | Tensile strength (MPa) | Elongation (%) | Thermal conductivity $(W/(mK)^{-1})$ |
|---|---|---|---|---|---|---|---|---|---|
| AA 5754 | Bal. | 3.1 | 0.5 | 0.2 | 0.4 | 0.4 | 258 | 23.5 | 147 |
| Mg AZ31 | 2.9 | bal. | 0.3 | 1.1 | – | 0.01 | 260 | 22.5 | 96 |

heat balance at both sides. The welding assembly and configurations of electrodes are shown schematically in Fig. 1. The welding duration (weld time: 5 cycles; downslope time: 70 cycles) and welding force (4 kN) were kept constant for the welding procedures. The coupons were welded with welding currents from 16 kA to 42 kA. The microstructures of the weld samples were examined by optical microscopy (OM), scanning electron microscopy (SEM) equipped with energy dispersive X-ray analysis (EDS) and X-ray diffraction (XRD). At least three tensile shear specimens were prepared for each condition to evaluate the mechanical properties. After testing, the fracture surfaces were investigated with SEM and EDS.

## 3. Results and discussion

### 3.1. Nugget Shape

Fig. 2 shows an optical micrograph taken from a cross-section of an Al/Mg weld with Ni interlayer using a welding current of 32 kA. The Ni interlayer remained un-melted during the welding process due to significantly higher melting point of nickel (1453 °C) compared to those of magnesium and aluminum alloys (650 °C and 660.3 °C). The reaction between Mg and Al alloys was completely prevented since they remained separated during the welding. However the thickness of the interlayer was reduced by approximately 20 μm in the central part of the weld. This is due to dissolution of nickel into the molten pools of Mg and Al as shown in the microstructural analysis later in Section 3.2. Fig. 3 shows the dependence of nugget diameter (measured on the Mg and Al sides) on the applied welding current. In general, the nugget produced at the Mg/Ni interface was larger than the one at the Al/Ni interface. This is possibly due to the differences such as thermal and electrical properties and even density between Mg and Al alloys.

The AA5754 has higher thermal conductivity than that of AZ31 ($K_{AZ31} = 96$ W/m K and $K_{AA5754} = 147$ W/m K at ambient temperature [18]), and lower electrical resistivity than that of AZ31 ($\rho_{AZ31} = 92$ nΩ m and $\rho_{AA5754} = 49$ nΩ m at ambient temperature [18]). Both lower resistance and higher conductivity might result in lower heat generation and higher heat dissipation, and hence smaller nugget at Al side. The required energy for melting the same volume of Mg and Al was compared in previous study [20]. Because the density

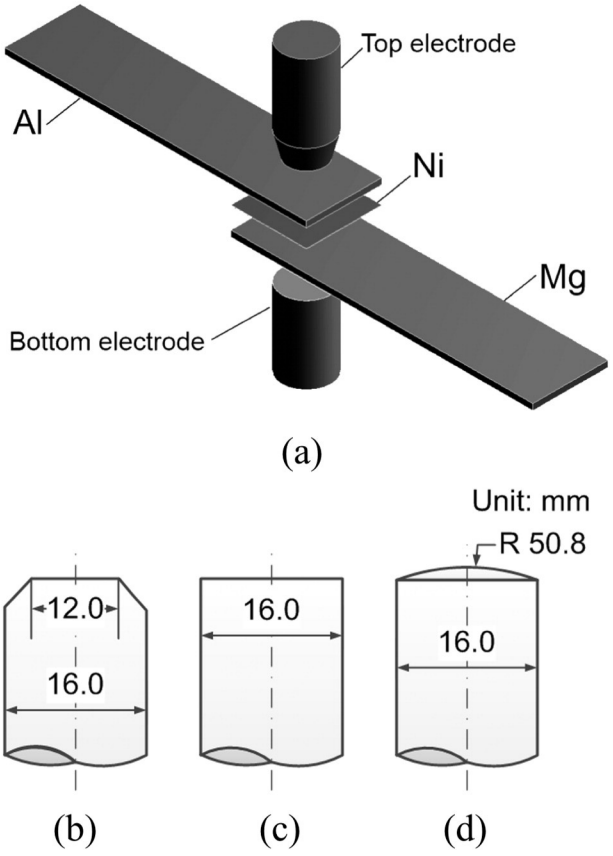


**Fig. 1.** Schematic illustration: (a) welding assembly for RSW using Ni interlayer; (b) modified electrode at Al side; (c) modified electrode at Mg side; (d) original FF-25 domed electrode used in Ref. [15].

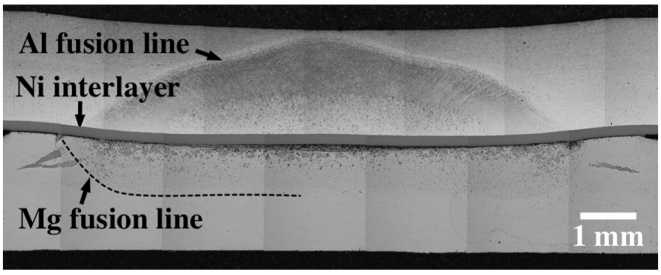


**Fig. 2.** Typical nugget of dissimilar Al/Mg joint using Ni interlayer.

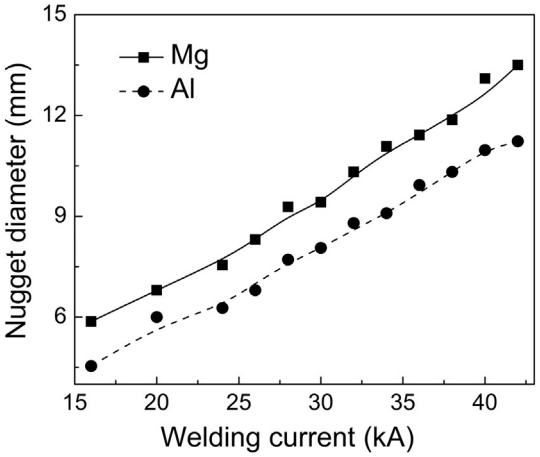


**Fig. 3.** Nugget diameter vs. welding current (with Ni interlayer).

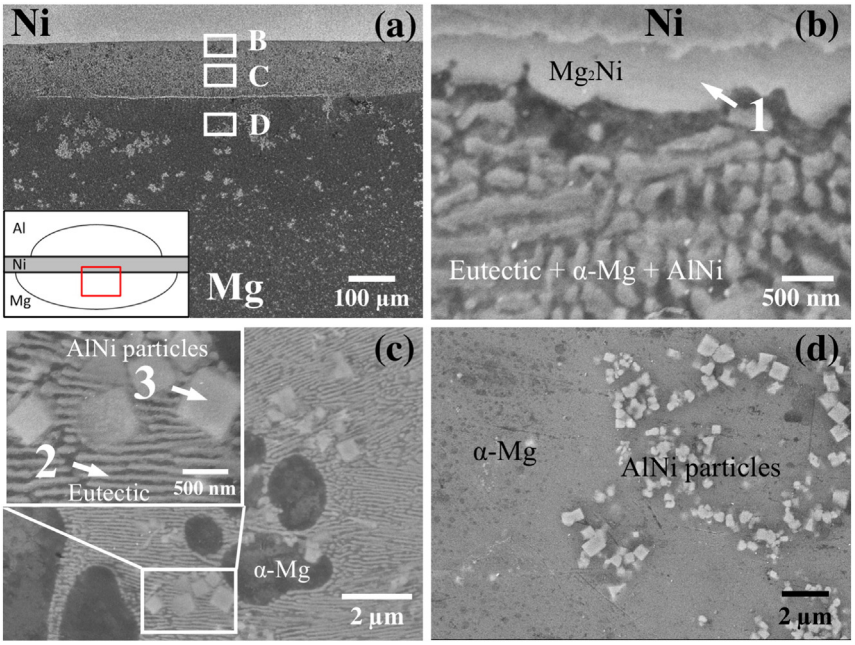


**Fig. 4.** (a) Mg/Ni interfacial region in the center of nugget (welding current: 32 kA) and highly magnified micrographs of area B (b), C (c) and D (d) as highlighted in (a); a $Mg_2Ni$ reaction layer, the lamellar structure (Mg–$Mg_2Ni$ eutectic + α-Mg + AlNi) and AlNi particles were observed at the interfacial region.

**Table 2**
EDS analysis results (at.%) for the highlighted regions shown in Figs. 4 and 9.

| Spectrum | Percentage composition (at.%) | | | Possible phases based on Al/Ni and Mg/Ni phase diagrams |
|---|---|---|---|---|
| | Mg | Al | Ni | |
| 1 | 72.6 | 0.3 | 27.1 | $Mg_2Ni$ |
| 2 | 80.4 | – | 19.6 | Mg–$Mg_2Ni$ eutectic |
| 3 | 19.3 | 39.5 | 41.2 | AlNi + Mg–$Mg_2Ni$ eutectic |
| 4 | – | 76.4 | 23.6 | $Al_3Ni$ |
| 5 | 1.7 | 89.7 | 8.6 | Al–$Al_3Ni$ eutectic |

of Mg is 1.7 g/cm$^3$, which is about 1/3 lower than that of Al (2.7 g/cm$^3$), the energy needed for melting Mg was 42% less than that for Al. So even same amount of heat was applied on the specimens, Mg would melt much more in volume.

Penner et al.'s attempt to join magnesium to aluminum with a Ni interlayer using the RSW process was unsuccessful since no reaction layer was formed at the Al/Ni interface [15]. This could be because the heat generated during welding was too low (applied welding currents in Penner's study were between 16 and 24 kA), so no metallurgical reaction occurred at the Al/Ni interface. A successful metallurgical reaction would take place in a liquid/solid couple if the liquid metal completely wets the solid substrate [21]. Since the welding current was too low, the heat required for surface melting of aluminum might

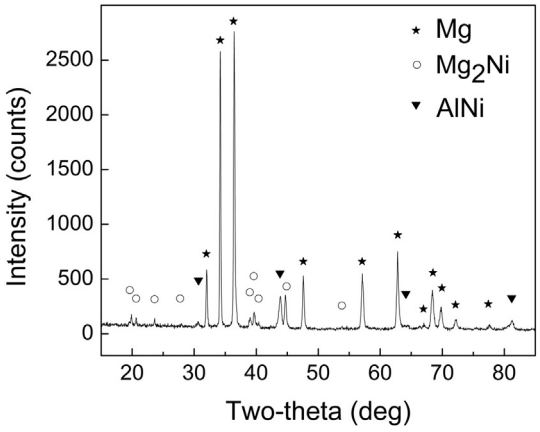


**Fig. 6.** XRD patterns taken from fracture surface on the Mg side of the nugget.

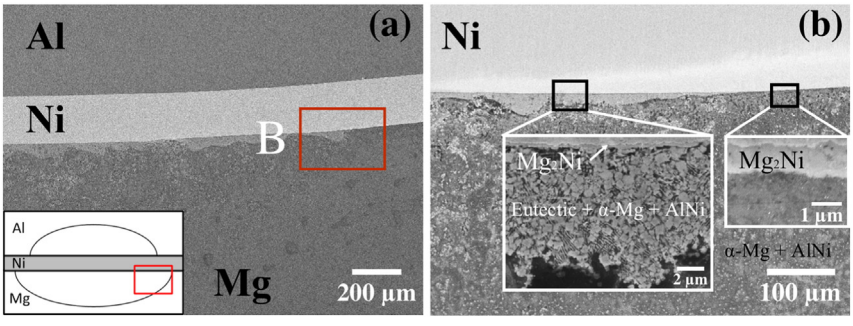


**Fig. 5.** (a) Mg/Ni interfacial region at the edge of nugget (welding current: 32 kA) and highly magnified micrograph of area B (b) as highlighted in (a).

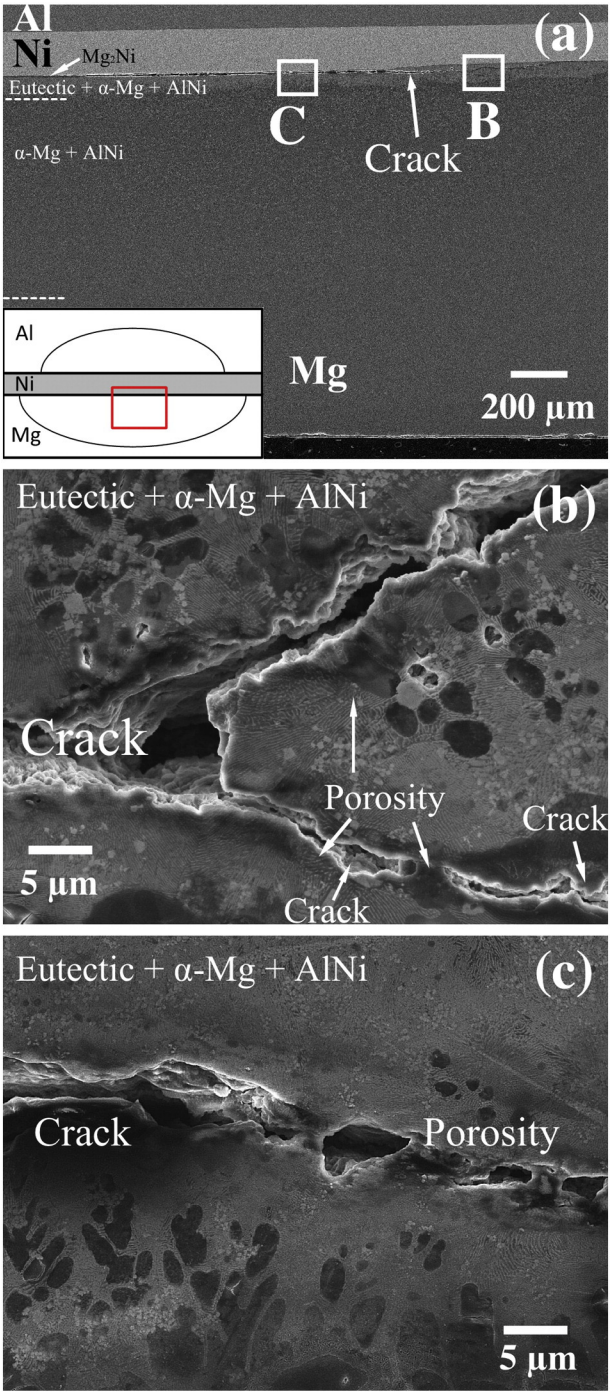


**Fig. 7.** (a) Mg/Ni interfacial region in the center of nugget (welding current: 42 kA) and highly magnified micrographs of area B (b), C (c) as highlighted in (a).

not be sufficient in Ref. [15]. Also a great proportion of the generated heat might dissipate through the Al base metal due to its high thermal conductivity. Therefore, wetting of the Ni solid interlayer could be very poor and continuous formation of the reaction layer at the Al/Ni interface did not take place. Penner et al. confirmed that no joining occurred between Al sheet and Ni interlayer after welding [15].

In the current study, however, since the electrode with smaller tip face diameter was utilized for the Al side, even at low welding currents (26 kA), consistent metallurgical reaction occurred at the Al/Ni interface.

### 3.2. Microstructural observations

#### 3.2.1. Microstructure of Mg/Ni interface

Fig. 4a shows a typical microstructure of the Mg/Ni interface at the centre of a nugget (welding current: 32 kA). The microstructure changed from the top (Ni side) to bottom (Mg side) of the fusion zone. Fig. 4b, c and d shows magnified microstructures at the regions highlighted in Fig. 4a. A sub-micron layer with a thickness of around 600 nm was found continuously along the Mg/Ni interface (Fig. 4b) enriched in Mg and Ni (Spectrum 1 in Table 2). The microstructure below the submicron layer was composed of lamellar structure (enriched by Ni and Mg) along with isolated diamond-shaped particles (enriched by Al and Ni) as shown in Fig. 4c and Spectra 2 and 3 in Table 2. Such microstructure developed continuously through the Mg fusion zone up to a distance of ~120 μm away from the interface. The IMC particles were still observed as much as 350 μm away from the interface (Fig. 4d).

Fig. 5a shows the microstructure of the Mg/Ni interface at the edge region of the nugget. Fig. 5b shows magnified microstructure at the region highlighted in Fig. 5a. The lamellar structure had inconsistent thickness in this region and disappeared at the end of the nugget.

The X-ray diffraction analysis (XRD) was carried out to characterize the phases at the Mg/Ni interface, because the dimensions of the phases were too small for accurate EDS analysis. Based on the XRD analysis (Fig. 6) and the EDS results (Table 2), the reaction submicron layer at the Mg/Ni interface was characterized as $Mg_2Ni$, the lamellar structure was Mg–$Mg_2Ni$ eutectic + α-Mg + AlNi particles, and the sub-layer was α-Mg + AlNi particles respectively.

During the welding process using intermediate welding currents, Mg was melted and wet the surface of the Ni interlayer. Thus, Ni atoms diffused in Mg liquid. Dissolution of transition metals such as nickel, in liquid metals is a diffusion-controlled process [22–24]. The diffusion penetration depth is dependent on the diffusivity coefficient of the diffused atom in the medium and time. Therefore a diffusion gradient existed from Mg–Ni interface toward the un-melted Mg.

During cooling in the center of the nugget, Al atoms in the Mg AZ31 alloy dissolved in the Mg liquid reacted with the diffused Ni atoms, forming AlNi compound as diamond-shaped particles as shown typically in Fig. 4c and d. Due to total consumption of Al and Ni via Al–Ni reaction, solidification in the region farther away from Mg/Ni interface was completed by formation of α-Mg (Fig. 4d). Within the region adjacent to the Mg–Ni interface, the concentration of Ni atoms was higher. Thus, even after the complete consumption of dissolved Al via Al–Ni reaction, the concentration of Ni was still high enough so the Mg–Ni reaction occurred. A thin liquid layer, directly in contact with the Ni interlayer, was enriched beyond the eutectic composition range and therefore formed $Mg_2Ni$ (Fig. 4b). Solidification at the Mg/Ni interfacial region was completed by the eutectic reaction: $L \rightarrow \alpha\text{-Mg} + Mg_2Ni$ (Fig. 4c). The presence of Mg–$Mg_2Ni$ eutectic as well as AlNi phase has been previously confirmed at the Mg/Ni interface [17,21,25–27].

Fig. 7a shows the Mg/Ni interfacial region within the center of a typical nugget produced using high welding current (42 kA). It was evident as shown by comparison of Figs. 4a and 7a that using the high welding current deteriorated the microstructure at the interface. Large cracks existed in the lamellar structure close to the Mg/Ni interface. Fig. 7b and c shows magnified microstructures at the regions highlighted in Fig. 7a. Heavy cracks and porosity were found in the lamellar structure. The heavy evaporation of the element Mg at the Mg/Ni interface has been shown to increase the probability of porosity [28–30], related to the high heat input with 42 kA welding current. Shrinkage voids have been suggested to be one of the main defects in resistance spot welding of magnesium alloys [31]. During welding by high currents (such as 42 kA in this study), liquid pressure inside the nugget intensified [32]. Since the nugget edges were not fully clamped by the electrodes, expulsion occurred, resulting in loss of liquid within the fusion zone. Liquid adjacent to the submicron layer was the last to solidify. Thus, shrinkage

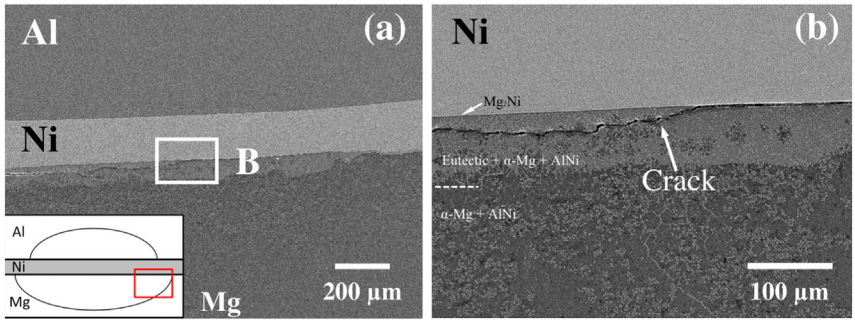


**Fig. 8.** (a) Mg/Ni interfacial region at the edge of nugget (welding current: 42 kA) and highly magnified micrograph of area B (b) as highlighted in (a).

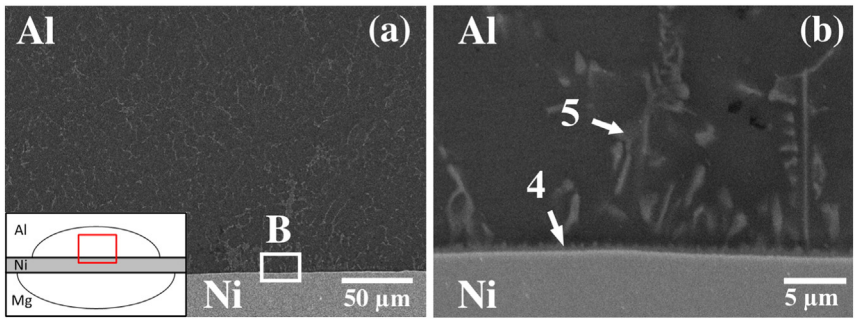


**Fig. 9.** (a) Al/Ni interfacial region (welding current: 32 kA); (b) highly magnified micrograph of area B in (a); a continuous $Al_3Ni$ reaction layer and Al–$Al_3Ni$ eutectic structure were observed at the interfacial region.

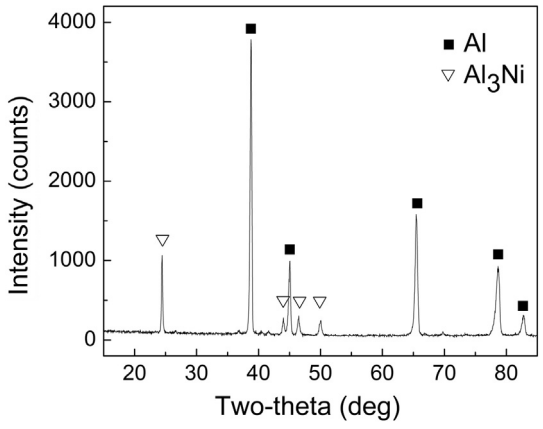


**Fig. 10.** XRD patterns taken from fracture surface on the Al side of the nugget.

stresses were intensified in the lamellar structure adjacent to the $Mg_2Ni$ submicron layer of the nugget. Consequently, cracking occurred extensively in the nugget. Porosity defects may also facilitate the crack initiation [33]; Fig. 7b and c shows porosity at the crack initiation location. In addition, based on the great difference between Mg and Ni in thermal expansion coefficient, the internal stress would be high under the rapid heating and cooling rate during welding. This is another potential cause of cracking at the Mg/Ni interfacial region [29,34].

Fig. 8a shows the microstructure at the edge of a nugget at the Mg/Ni interfacial region using high welding current (42 kA). Fig. 8b shows the magnified microstructure at the region highlighted in Fig. 8a. The lamellar structure still existed at the edge of the nugget with a thickness around 60 μm, which was different from the case at a welding current of 32 kA (Fig. 5b). Cracks also could be found at the edge of the nugget in the lamellar structure region.

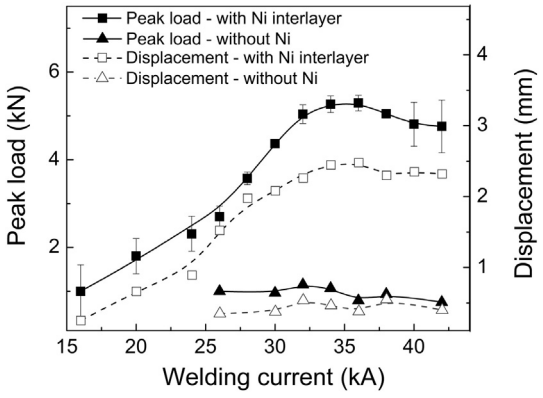


**Fig. 11.** Peak load and displacement vs. welding current for the joints with and without Ni interlayer.

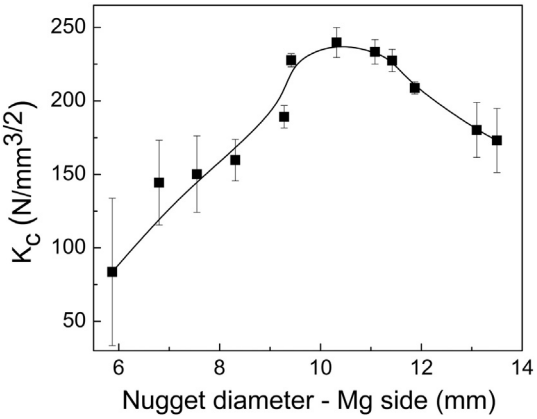


**Fig. 12.** Critical stress intensity ($K_C$) vs. nugget diameter in Mg.

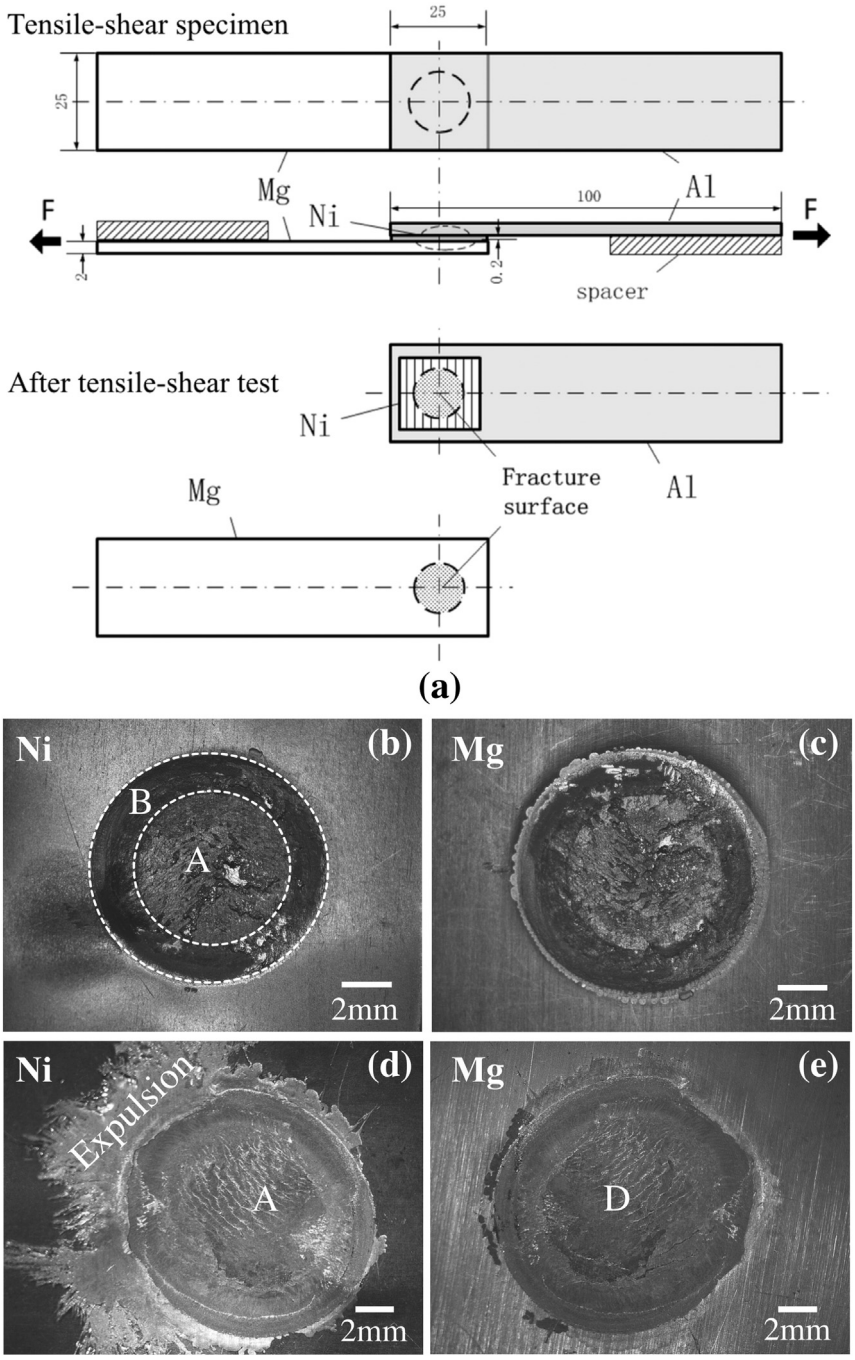


**Fig. 13.** (a) schematic of tensile shear specimen and fracture surfaces; fracture surface of nugget on Ni (Al) and Mg side at welding current of 32 kA ((b) and (c)) and 42 kA ((d) and (e)).

*3.2.2. Microstructure of Al/Ni interface*

Fig. 9a shows a typical microstructure within the central region of the nugget at the Al/Ni interface (welding current: 32 kA). Fig. 9b shows magnified microstructures at the region highlighted in Fig. 9a. A continuous sub-micron layer and Al–Ni eutectic structure (enriched in Al and Ni as shown in Table 2 Spectra 4 and 5) were formed at the interfacial region. The edge region of the nugget had the same morphology as in the central region. The Al–Ni bonding interface was separated by force to analyze the phases on the Al/Ni interface. Based on X-ray diffraction analysis (Fig. 10) and the EDS results (Table 2), the reaction submicron layer at Al/Ni interface was characterized as $Al_3Ni$ compound and beyond $Al_3Ni$ layer was Al–$Al_3Ni$ eutectic structure. Previous investigations have confirmed the formation of $Al_3Ni$ IMC layer at the Al/Ni interface [26,35–37].

During welding, the surface of aluminum was melted and reacted with solid nickel interlayer. This also caused the dissolution of Nickel into the aluminum liquid. Within the region adjacent to the Al/Ni interface, the concentration of Ni was higher. Thus, a thin $Al_3Ni$ reaction layer was formed by the Al–Ni reaction ($L \rightarrow Al_3Ni$) at the beginning of solidification. In the region far away from the Al/Ni interface, solidification was completed by the formation of α-Al ($L \rightarrow$ α-Al) with absence of Ni. Finally, the solidification of the remaining Ni-containing liquid was completed by the eutectic reaction ($L \rightarrow$ α-Al + $Al_3Ni$) at the region adjacent to the $Al_3Ni$ reaction layer. No obvious microstructure

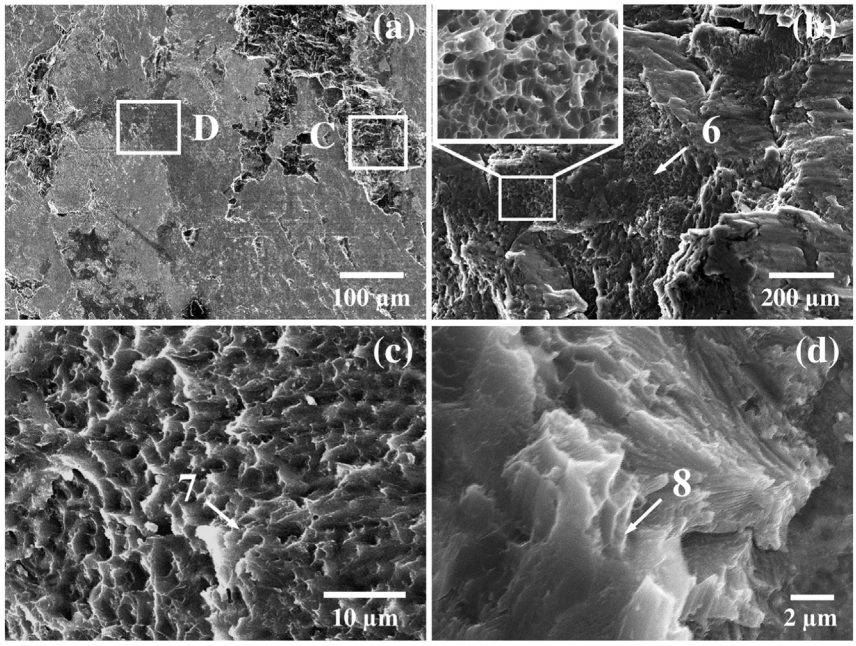


**Fig. 14.** Fracture surface on Ni side at 32 kA welding current: (a) and (b) areas A and B in Fig. 13b; (c) and (d) highly magnified micrographs taken from area C and D in (a); (a), (c) and (d) show the failure occurred in the lamellar structure (Mg–$Mg_2Ni$ eutectic + α-Mg + AlNi) in the central region of the nugget; (b) shows the failure occurred in the α-Mg fusion zone at the edge of the nugget.

deterioration was found at the Al/Ni interfacial region when high welding current (42 kA) was applied.

### 3.3. Mechanical properties

Fig. 11 plots the tensile shear peak load and displacement of the nuggets produced by different welding currents. For all the applied welding currents, a joint produced by insertion of a Ni interlayer was substantially stronger than a direct joint. The displacement-to-failure was extremely low in the direct Al/Mg joint. This indicated the brittle nature of the direct joint due to the formation of Mg–Al compounds, as already reported in literatures [2,3,5,6,8,38,39]. Insertion of a nickel interlayer between Al and Mg base metals successfully prevented direct contact between Mg and Al melts during welding. Therefore, formation of brittle Mg–Al IMCs was avoided. The peak load values obtained from the welds with Ni interlayer produced by welding currents of 32–36 kA were close to those reported for the AZ31/AZ31 spot welds [40–43]. This comparison indicated that a high joint efficiency was achieved via using the Ni interlayer. Up to intermediate nugget diameters (Fig. 3), the peak load increased with increase of the welding current. Such results are as expected, since the stress intensity at the spot weld notch decreased with growth in the nugget diameter.

**Table 3**
EDS analysis results (at.%) for the highlighted regions shown in Figs. 14 and 15.

| Spectrum | Percentage composition (at.%) | | | Possible phases based on Al/Ni and Mg/Ni phase diagrams |
|---|---|---|---|---|
| | Mg | Al | Ni | |
| 6 | 100 | – | – | Mg |
| 7 | 98.2 | 1.5 | 0.3 | Mg |
| 8 | 83.9 | 2.2 | 13.9 | Mg + Mg–$Mg_2Ni$ eutectic + AlNi |
| 9 | 80.1 | 6.9 | 13 | Mg + Mg–$Mg_2Ni$ eutectic + AlNi |
| 10 | 94.5 | – | 5.5 | Mg + Mg–$Mg_2Ni$ eutectic |

In order to normalize the effect of nugget diameter, the critical stress intensity ($K_C$) at the spot weld notch was calculated. Due to the fact that the loading condition at a spot weld was usually multiaxial, mode I, II and III stress intensities were all considered in Zhang's solution for spot weld lap shear specimens [44]:

$$K_C = 0.694 \frac{F_t}{d\sqrt{t}} \quad (1)$$

where $F_t$ is the peak tensile load, t is the sheet thickness and d is the nugget diameter. Mg side nugget diameters (Fig. 3) were used in this calculation, since the failures of the tested specimens occurred at the Mg/Ni interface region. Fig. 12 plots the $K_C$ values vs. nugget diameter. A sharp increase in $K_C$ value occurred for nugget diameter of 9.3 mm, up to 72% of the value compared to Mg–Mg similar welding at the same nugget size [41]. However, a drop in $K_C$ value occurred for nugget diameters larger than 11 mm. The reason for this sharp decrease will be discussed later in this paper.

Fig. 12 shows that the critical stress intensity was very low when low welding current was applied (nugget diameter < 9.3 mm as shown in Fig. 12). The microscopic observations on small nuggets revealed the frequent disappearance of the submicron Mg/Ni reaction layer at the edge of the nugget. Due to low heat generation at the Mg/Ni interface (using low welding current), metallurgical reactions were incomplete leading to the formation of a discontinuous layer. From the aforementioned statements, it can be inferred that the high joint strength of the nuggets produced by intermediate welding currents (32–36 kA) was due to the continuous formation of submicron reaction layers at Al/Ni and Mg/Ni interfaces.

### 3.4. Fracture characteristics of the welds

All the welded samples failed at the Mg/Ni interface after tensile shear tests (Fig. 13a). Since the joint area at the Mg/Ni interface was larger than that of Al/Ni interface, it is concluded that the bonding between Al and Ni was stronger than that of Mg and Ni. Fig. 13b and c shows the fracture surfaces on Ni (Al) and Mg side of a nugget produced

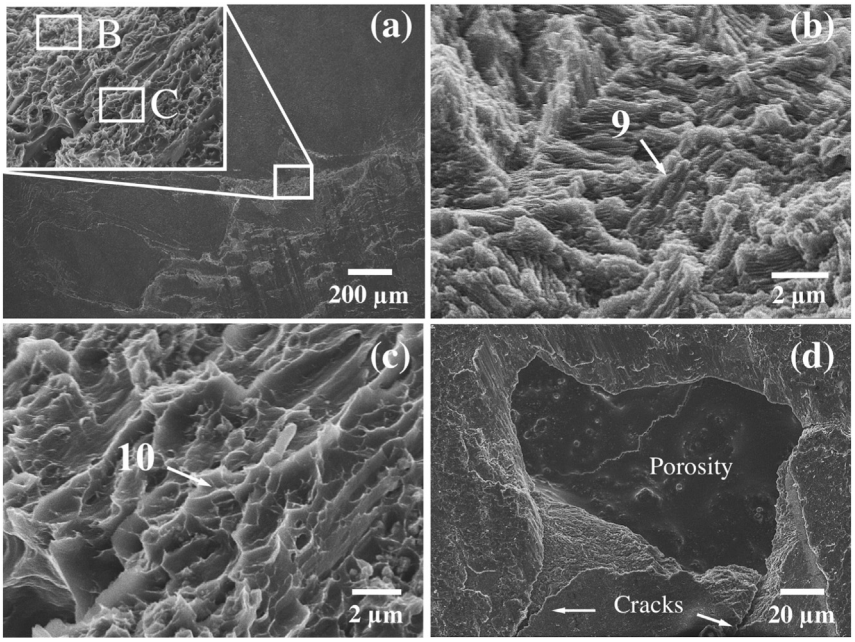


**Fig. 15.** Fracture surface on Ni side at 42 kA welding current: (a) taken from area A in Fig. 13d; (b) and (c) highly magnified micrographs taken from area B and C in (a); (d) area D in Fig. 13e; (a), (b) and (c) show the failure occurred in the lamellar structure (Mg–$Mg_2Ni$ eutectic + α-Mg + AlNi) of the whole joint; (d) shows the defects on the fracture surface.

by an intermediate welding current (32 kA), after the tensile shear test. It is clear that no expulsion occurred during welding. Fracture surfaces on Ni (Al) and Mg side of a nugget produced by high current (i.e. 42 kA) were different as shown typically in Fig. 13d and e. Expulsion occurred at high welding current.

Fig. 14 shows the microstructure of the fracture surface on the Ni side at intermediate welding current (32 kA). Fig. 14a shows the morphology in the central region of the fracture surface (Region A in Fig. 13b). The highly magnified microstructure of the highlighted region C (Fig. 14c) in Fig. 14a shows ductile fracture. Based on the EDS result (Spectrum 7 in Table 3), the ductile fracture occurred through the Mg phase. Brittle fracture was found in Region D (Fig. 14d) of Fig. 14a. The EDS result of Region D (Spectrum 8 in Table 3) shows that the failure occurred through the poor ductility Mg–$Mg_2Ni$ eutectic [45]. The edge region of the fracture surface (Regine B in Fig. 13b) shows a ductile fracture morphology in material rich in Mg (Fig. 14b and Spectrum 6 in Table 3). Based on the microstructure investigation of the Mg/Ni interface (Section 3.2.1) and the SEM/EDS results from the fracture surface (Fig. 14 and Table 3), the failure occurred in the lamellar structure (Mg–$Mg_2Ni$ eutectic + α-Mg + AlNi) in the central region of the nugget, and in the α-Mg fusion zone at the edge of the nugget.

Fig. 15 shows the microstructure of the fracture surface produced by the high welding current (42 kA). Fig. 15a shows a typical morphology of the whole fracture surface on the Ni side (Region A in Fig. 13d). Brittle fracture in a zone rich in Mg and Ni elements (Fig. 15b and Spectrum 9 in Table 3) was revealed by investigation of highlighted area B in Fig. 15a. Area C in Fig. 15a shows the ductile fracture that occurred through the Mg phase (Fig. 15c and Spectrum 10 in Table 3). The failure of the whole joint occurred in the lamellar structure (Mg–$Mg_2Ni$ eutectic + α-Mg + AlNi) at high welding current (42 kA). Fig. 15d shows the highly magnified microstructure of the region D in Fig. 13e. Porosity and cracks were found on the Mg side fracture surface. Defects were also observed in the lamellar structure at the Mg/Ni interface in the as-welded specimen using high welding current (Figs. 7 and 8). The oxidation at high temperature (Fig. 15b) may also contribute to the poor strength. These observations implied that early fracture in the tensile test of a nugget produced by high welding current was due to microstructure deterioration at the Mg/Ni interface. Therefore, fracture occurred more readily in the nuggets produced at high welding currents than the ones produced by intermediate welding currents.

## 4. Conclusions

This work has been concerned with the dissimilar joining of magnesium AZ31 to aluminum AA5754 with commercial pure Ni interlayer. The following conclusions have been drawn:

1. Strong joints were achieved using a pure nickel interlayer, which caused continuous Mg–Ni and Al–Ni intermetallic layers to form at Mg/Ni and Al/Ni interfaces respectively and prevent formation of the Al–Mg brittle intermetallic compounds.
2. Increasing welding current increased the nugget diameter and hence the joint strength when the current is up to 36 kA. But defects such as cracks and porosity formed in the Mg/Ni interfacial region when excessively high welding current (42 kA) was applied. This microstructure deterioration led to early fracture at the Mg/Ni interfacial region and the reduction in the joint strength.

## Acknowledgments

This research was supported by the Natural Sciences and Engineering Research Council (NSERC) of Canada, NSERC Magnesium Network (MagNET), and the State Scholarship Fund of China (No. 201206120134). The authors want to thank Professor S. Lawson for his discussion in this work, and Dr. P. Peng for his help on the EDS analysis.

## References

[1] M.W. Andure, S.C. Jirapure, L.P. Dhamande, Advance automobile material for light weight future – a review, IJCA Proceedings on International Conference on Benchmarks in Engineering Science and Technology 2012 ICBEST 2012, pp. 15–22.
[2] F. Hayat, The effects of the welding current on heat input, nugget geometry, and the mechanical and fractural properties of resistance spot welding on Mg/Al dissimilar materials, Mater. Des. 32 (2011) 2476–2484.
[3] V. Firouzdor, S. Kou, Al-to-Mg friction stir welding: effect of material position, travel speed, and rotation speed, Metall. Mater. Trans. A 41 (2010) 2914–2935.
[4] H.M. Rao, W. Yuan, H. Badarinarayan, Effect of process parameters on mechanical properties of friction stir spot welded magnesium to aluminum alloys, Mater. Des. 66 (2015) 235–245.

[5] Y.S. Sato, S.H.C. Park, M. Michiuchi, H. Kokawa, Constitutional liquation during dissimilar friction stir welding of Al and Mg alloys, Scr. Mater. 50 (2004) 1233–1236.
[6] L.M. Liu, H.Y. Wang, Z.D. Zhang, The analysis of laser weld bonding of Al alloy to Mg alloy, Scr. Mater. 56 (2007) 473–476.
[7] G. Mahendran, V. Balasubramanian, T. Senthilvelan, Developing diffusion bonding windows for joining AZ31B magnesium–AA2024 aluminium alloys, Mater. Des. 30 (2009) 1240–1244.
[8] Y. Luo, J. Li, Analysis of nugget formation during resistance spot welding on dissimilar metal sheets of aluminum and magnesium alloys, Metall. Mater. Trans. A 45 (2014) 5107–5113.
[9] P. Penner, L. Liu, A. Gerlich, Y. Zhou, Dissimilar resistance spot welding of aluminum to magnesium with Zn-coated steel interlayers, Weld. J. 93 (2014) 225S–231S.
[10] X.-D. Qi, L.-M. Liu, Fusion welding of Fe-added lap joints between AZ31B magnesium alloy and 6061 aluminum alloy by hybrid laser–tungsten inert gas welding technique, Mater. Des. 33 (2012) 436–443.
[11] L.M. Zhao, Z.D. Zhang, Effect of Zn alloy interlayer on interface microstructure and strength of diffusion-bonded Mg–Al joints, Scr. Mater. 58 (2008) 283–286.
[12] M. Gao, S. Mei, X. Li, X. Zeng, Characterization and formation mechanism of laser-welded Mg and Al alloys using Ti interlayer, Scr. Mater. 67 (2012) 193–196.
[13] L. Liu, X. Liu, S. Liu, Microstructure of laser-TIG hybrid welds of dissimilar Mg alloy and Al alloy with Ce as interlayer, Scr. Mater. 55 (2006) 383–386.
[14] G. Song, G. An, L. Liu, Effect of gradient thermal distribution on butt joining of magnesium alloy to steel with Cu–Zn alloy interlayer by hybrid laser–tungsten inert gas welding, Mater. Des. 35 (2012) 323–329.
[15] P. Penner, L. Liu, A. Gerlich, Y. Zhou, Feasibility study of resistance spot welding of dissimilar Al/Mg combinations with Ni based interlayers, Sci. Technol. Weld. Join. 18 (2013) 541–550.
[16] L.M. Liu, L.M. Zhao, R.Z. Xu, Effect of interlayer composition on the microstructure and strength of diffusion bonded Mg/Al joint, Mater. Des. 30 (2009) 4548–4551.
[17] H. Wang, L. Liu, F. Liu, The characterization investigation of laser-arc-adhesive hybrid welding of Mg to Al joint using Ni interlayer, Mater. Des. 50 (2013) 463–466.
[18] Y. Zhang, Z. Luo, Y. Li, Z. Liu, Z. Huang, Microstructure characterization and tensile properties of Mg/Al dissimilar joints manufactured by thermo-compensated resistance spot welding with Zn interlayer, Mater. Des. 75 (2015) 166–173.
[19] Committee AIH, ASM Handbook Volume 2, Properties and Selection: Nonferrous Alloys and Special Purpose Materials. ASM International, 1995.
[20] D.C. Wagner, Y.K. Yang, S. Kou, Spatter and Porosity in Gas–Metal Arc Welding of Magnesium Alloys: Mechanisms and Elimination, Weld. J. 92 (2013) 347s–362s.
[21] A.M. Nasiri, D.C. Weckman, Y. Zhou, Interfacial microstructure of diode laser brazed AZ31B magnesium to steel sheet using a nickel interlayer, Weld. J. 92 (2013) 1s–10s.
[22] A.J. Hickl, R.W. Heckel, Kinetics of phase layer growth during aluminide coating of nickel, Metall. Trans. A 6 (1975) 431–440.
[23] V.I. Dybkov, Interaction of iron–nickel alloys with liquid aluminium, J. Mater. Sci. 28 (1993) 6371–6380.
[24] V.N. Yerembnko, Y.V. Natanzon, V.I. Dybkov, Interaction of the refractory metals with liquid aluminium, J. Less Common Met. 50 (1976) 29–48.
[25] A.M. Nasiri, P. Chartrand, D.C. Weckman, N.Y. Zhou, Thermochemical analysis of phases formed at the interface of a Mg alloy–Ni-plated steel joint during laser brazing, Metall. Mater. Trans. A 44 (2012) 1937–1946.
[26] C.L. Tsao, S.W. Chen, Interfacial reactions in the liquid diffusion couples of Mg/Ni, Al/Ni and Al/(Ni)–Al2O3 systems, J. Mater. Sci. 30 (1995) 5215–5222.
[27] X. Qi, G. Song, Interfacial structure of the joints between magnesium alloy and mild steel with nickel as interlayer by hybrid laser-TIG welding, Mater. Des. 31 (2010) 605–609.
[28] C.W. Tan, L.Q. Li, Y.B. Chen, A.M. Nasiri, Y. Zhou, Microstructural characteristics and mechanical properties of fiber laser welded-brazed Mg alloy-stainless steel joint, Weld. J. 93 (2014) 399–409.
[29] Y. Miao, D. Han, J. Yao, F. Li, Effect of laser offsets on joint performance of laser penetration brazing for magnesium alloy and steel, Mater. Des. 31 (2010) 3121–3126.
[30] L. Liu, S.Q. Zhou, Y.H. Tian, J.C. Feng, J.P. Jung, Y.N. Zhou, Effects of surface conditions on resistance spot welding of Mg alloy AZ31, Sci. Technol. Weld. Join. 14 (2009) 356–361.
[31] H. Luo, C. Hao, J. Zhang, Z. Gan, H. Chen, H. Zhang, Characteristics of resistance welding magnesium alloys AZ31 and AZ91, Weld. J. 90 (2011) 249–257.
[32] J. Senkara, H. Zhang, Cracking in spot welding aluminum alloy AA5754, Weld. J. 79 (2000) 194S–201S.
[33] H. Mayer, M. Papakyriacou, B. Zettl, S.E. Stanzl-Tschegg, Influence of porosity on the fatigue limit of die cast magnesium and aluminium alloys, Int. J. Fatigue 25 (2003) 245–256.
[34] Y.G. Miao, D.F. Han, J.Z. Yao, F. Li, Microstructure and interface characteristics of laser penetration brazed magnesium alloy and steel, Sci. Technol. Weld. Join. 15 (2010) 97–103.
[35] J.F. Zhao, C. Unuvar, U. Anselmi-Tamburini, Z.A. Munir, Kinetics of current-enhanced dissolution of nickel in liquid aluminum, Acta Mater. 55 (2007) 5592–5600.
[36] J. Zhao, C. Unuvar, U. Anselmi-Tamburini, Z.A. Munir, Microstructural evolution during the dissolution of nickel in liquid aluminum under the influence of an electric field, Acta Mater. 56 (2008) 1840–1848.
[37] K.O. Cooke, T.I. Khan, G.D. Oliver, Transient liquid phase diffusion bonding Al-6061 using nano-dispersed Ni coatings, Mater. Des. 33 (2012) 469–475.
[38] L. Liu, D. Ren, A novel weld-bonding hybrid process for joining Mg alloy and Al alloy, Mater. Des. 32 (2011) 3730–3735.
[39] X. Dai, H. Zhang, J. Liu, J. Feng, Microstructure and properties of Mg/Al joint welded by gas tungsten arc welding-assisted hybrid ultrasonic seam welding, Mater. Des. 77 (2015) 65–71.
[40] L. Xiao, L. Liu, Y. Zhou, S. Esmaeili, Resistance-spot-welded AZ31 magnesium alloys: part I. dependence of fusion zone microstructures on second-phase particles, Metall. Mater. Trans. A 41 (2010) 1511–1522.
[41] L. Liu, L. Xiao, J.C. Feng, Y.H. Tian, S.Q. Zhou, Y. Zhou, Resistance spot welded AZ31 magnesium alloys, part II: effects of welding current on microstructure and mechanical properties, Metall. Mater. Trans. A 41 (2010) 2642–2650.
[42] S. Niknejad, L. Liu, M.-Y. Lee, S. Esmaeili, N.Y. Zhou, Resistance spot welding of AZ series magnesium alloys: Effects of aluminum content on microstructure and mechanical properties, Mater. Sci. Eng. A 618 (2014) 323–334.
[43] H. Shi, R. Qiu, J. Zhu, K. Zhang, H. Yu, G. Ding, Effects of welding parameters on the characteristics of magnesium alloy joint welded by resistance spot welding with cover plates, Mater. Des. 31 (2010) 4853–4857.
[44] S. Zhang, Stress intensities at spot welds, Int. J. Fract. 88 (1997) 167–185.
[45] K.H. Eckelmeyer, R.W. Hertzberg, The structure and mechanical behavior of the Mg–$Mg_2Ni$ eutectic composite, Metall. Trans. A 3 (1972) 609–616.